

# Radiation Pressure Induced Instabilities in Laser Interferometric Detectors of Gravitational Waves

A. Pai <sup>1</sup>, S. V. Dhurandhar <sup>1,2</sup>, P. Hello <sup>3</sup>, J-Y. Vinet <sup>3</sup>

<sup>1</sup> *Inter-University Centre for Astronomy and Astrophysics, Post Bag 4, Ganeshkhind, Pune 411007, India.*

<sup>2</sup> *Dept. of Physics and Astronomy, UWCC, PO Box 913, Cardiff CF2 3YB, Cardiff, U.K.*

<sup>3</sup> *Groupe Virgo, Laboratoire de l'Accélérateur Linéaire, Bat. 200, Centre d'Orsay, 91405 Orsay, France.*

The large scale interferometric gravitational wave detectors consist of Fabry-Perot cavities operating at very high powers ranging from tens of kW to MW for next generations. The high powers may result in several nonlinear effects which would affect the performance of the detector. In this paper, we investigate the effects of radiation pressure, which tend to displace the mirrors from their resonant position resulting in the detuning of the cavity. We observe a remarkable effect, namely, that the freely hanging mirrors gain energy continuously and swing with increasing amplitude. It is found that the ‘time delay’, that is, the time taken for the field to adjust to its instantaneous equilibrium value, when the mirrors are in motion, is responsible for this effect. This effect is likely to be important in the optimal operation of the full-scale interferometers such as VIRGO and LIGO.

04.80.Nn Gravitational wave detectors and experiments, 42.65.Sf Dynamics of nonlinear optical systems, 42.60.Da Resonators, cavities, amplifiers, arrays, and rings

## I. INTRODUCTION

The general theory of relativity predicts the existence of gravitational waves. Since gravity couples very weakly to matter, highly sensitive detectors are required to detect gravitational waves. Over the next decade several large-scale interferometric gravitational wave detectors will come on-line. These include the LIGO, composed of two interferometric detectors situated in the United States each with baselines of 4 km, VIRGO, an Italian/French project located near Pisa with a baseline of 3 km, GEO600, a British/German interferometer under construction near Hannover with a baseline of 600 m, TAMA in Japan, a medium-scale laser interferometer with a baseline of 300 m and with funding approval AIGO500, the proposed 500 m project sponsored by ACIGA [1–5]. The large scale interferometers will use Fabry-Perot cavities and the ground based detectors will have arm lengths of few kilometers. There are several noise sources which plague the detector. Amongst them, the photon shot noise is dominant at high frequencies. It is reduced by increasing the amount of power of the laser source, as the noise is inversely proportional to the square root of the power. Therefore the cavities envisaged will operate with very high powers in their arms, tens of kiloWatts for initial detectors and perhaps powers as high as megaWatts in planned advanced detectors. The high power stored in the cavities can generate a number of nonlinear effects which would adversely affect the operation of the optical cavity. Here, we look into one such effect, namely, the dynamics of mirrors under the radiation pressure force. In earlier literature, we and others had investigated the thermo-elastic deformation of the mirrors due to the absorption of the power in the coatings and performed a longitudinal analysis of the cavity [6–10]. Following these investigations, we studied the effects of radiation pressure in the cavity, in the regime when the displacement of the mirror is small compared with the line-width of the cavity, the cavity is servoed at resonance with a realistic servo control and the variation in the radiation pressure force is linearly dependent on the displacement [11]. The radiation pressure effects have also been investigated in earlier literature [12–16]. Here, however, since we now have a reasonably good idea about the instrumental parameters to be used in the large scale detectors, we expect that our analysis here will be important to the experimentalists. We assume that the mirrors are hanging ‘freely’ (there is no active servo control) and the radiation pressure exerts force on them which displaces them from resonance. It is very important for people involved in the experiments being built to have a quantitative idea of the magnitude of these effects. For instance, it would be necessary to take into account these effects and modify the servo transfer functions to be used for the control of the experiments.

The main result of this paper is to establish that the freely hanging mirrors continuously gain energy and swing with ever increasing amplitude when subjected to radiation pressure force arising from the light field. This result seems to be in opposition with the results of Meystre et al., who found in [12] a mirror confinement due to the radiation pressure. The reason for this difference of behaviour is the ‘time delay’ effect which is also examined in detail in this paper. The time delay is large for the long (kilometric) cavities, primarily studied here, while it can be neglected for short cavities such as the one studied by Meystre et al. [12] and those used in most of labs. Closed form expressions have been given which facilitate in understanding the physics of the phenomenon.

The paper is organized as follows:

In section II, we set up the equation of motion of the free mirrors. We examine the motion of the mirrors with the two forces (i) the radiation pressure force, (ii) the force of gravity. In section III, we numerically integrate the equations of motion using the so called ‘Phase Space Method’. We present the results for the particular case, when the mirrors are in the resonance positions and the laser is switched on. We observe that the amplitude of the motion of the mirrors increases with time and energy is pumped into the system. For very large times, when the amplitude of the system is also very large, so that the mirrors cross several of the Fabry-Perot resonances in one cycle of the pendulum, the motion approximates to that of an anti-damped harmonic oscillator. We give also, for comparison, the numerical results obtained for a short cavity : no anti-damping is exhibited in this case, in agreement with earlier results [12]. In section IV, we obtain analytically, under the quasi-static approximation, the phase space trajectories of the motion of the individual mirrors as well as the motion in the differential mode and the common mode (the centre of mass mode). The analytical results match with the numerical ones remarkably. In section V, we give a quantitative description of the phenomenon under the assumption that the velocity of the mirror does not change very much on the time scale of the storage time of the cavity. We find that the gain in energy is due to a differential radiation pressure force arising from the asymmetry, according as the mirrors are approaching each other or moving away from each other. We obtain approximate analytical expressions for the differential force, the time ‘delay’ and then proceed to compute the gain in energy per cycle when the mirrors encounter a single resonance or cross several resonances. For large amplitudes, when the mirrors cross several resonances, the system behaves like an anti-damped harmonic oscillator. We can then associate an effective negative  $Q$ -factor for the system. We show that the  $Q$ -factor depends on the input power, the finesse of the cavity and the round trip time of the cavity. Finally in section VI, we study the behaviour of the system when it is initially in equilibrium and goes out of lock. This may happen when the servo loop is suddenly opened.

## II. OPTICAL AND MECHANICAL EQUATIONS

We consider only ‘free’ mirrors meaning that no servo control loop is used. The only forces acting on the mirrors are the radiation pressure force and gravity which manifests itself as the restoring force of the pendulum. We consider a single cavity with mirrors  $M1$  and  $M2$  which are suspended as shown in fig.1. The input beam  $A$  enters the cavity from mirror  $M1$  and bounces back and forth between the two mirrors. After several round trips, whose number is of the order of the finesse of the cavity, the field builds up inside the cavity. The magnitude of the field depends on the finesse of the cavity, the input power and the detuning of the cavity. The field or the power produces the radiation pressure force which pushes on the mirrors, driving them apart, thus changing the distance between the two. This in turn changes the power inside the cavity. For instance, if the mirrors were hanging in a position of resonance, the radiation pressure force drives the cavity out of resonance, reducing the radiation pressure force. The mirrors start swinging with radiation pressure force adjusting to the continuously varying length of the cavity. It is found that the radiation pressure force does not adjust instantaneously to the new length but *lags* behind the expected static force given by the Fabry-Perot curve (the Airy function) by a time-lag comparable to the storage time of the cavity. The time-lag has been called ‘time delay’ in earlier literature [14].

The slowly varying amplitude of the field inside the cavity at time  $t$ , denoted by  $B(t)$  satisfies the following equation,

$$B(t) = t_1 A \exp[ikx_1(t)] + RB(t - \tau) \exp[ikL(t)], \quad (2.1)$$

where,  $x_i(t)$ ,  $r_i$  and  $t_i$ ,  $i = 1, 2$  are the positions, reflectivities and transmitivities of the mirrors  $M1$  and  $M2$  respectively;  $R = r_1 r_2$ ,  $k = 2\pi/\lambda$ , where  $\lambda$  is the wavelength of the laser light,  $\tau$  is the round trip time and

$$L(t) = 2x_2(t - \tau/2) - x_1(t) - x_1(t - \tau). \quad (2.2)$$

In case of the VIRGO cavity, the arm length  $L_0$  is 3 km, the round trip time  $\tau = 2L_0/c \sim 2 \times 10^{-5}$  seconds, where  $c$  is the speed of light. This equation provides an iterative relation between the field amplitude at time  $t$  to the field amplitude at time  $t - \tau$  and the positions of the mirrors. We investigate the following two situations:

1. The mirrors are hanging in the positions of resonance and the laser is switched on at the time  $t = t_0$ .
2. The mirrors are hanging in an equilibrium state with the radiation pressure force balancing the restoring force of the suspension.

Situation 1 represents a possible experiment. When the servo-control is not operating, the mirrors will be freely in motion. Then, when the laser is switched on, the radiation pressure will affect the motion of the mirrors. However, here, we mainly deal with the case (as given in 1), when the mirrors are initially at rest and in the resonance position. However, many of our analytical formulae, for example, that of ‘time-delay’ apply to more general situations. Situation 2 describes the case when the interferometer is already in operation. Now if the servo-control loop is suddenly opened, the system will tend to become unstable. This case is also investigated.

The equations of motion for the mirrors correspond to forced harmonic oscillator with the forcing term arising from the radiation pressure force. We first compute the radiation pressure forces on each mirror. For mirror  $M1$ , the radiation pressure force comprises of two terms, electric field due the input laser beam,  $A$  and the intra-cavity field  $B$  as shown in fig.1. The radiation pressure force on  $M1$  is,

$$F_1(t) = -\frac{2}{c}[R^2 P(t - \tau) - r_1^2 P_0], \quad (2.3)$$

where,  $P(t) = |B(t)|^2$ ,  $P_0 = |A|^2$  and  $c$  is the speed of light.  $r_i^2$  is the fraction of average number of photons reflected by  $i$  th mirror for  $i = 1, 2$  respectively.

For  $M2$ , the radiation pressure force is given by

$$F_2\left(t - \frac{\tau}{2}\right) = \frac{2r_2^2}{c}P(t - \tau). \quad (2.4)$$

The equations of motion for the mirrors with the masses, natural frequencies and damping constants,  $m_i$ ,  $\omega_i$ ,  $\tau_i$ ;  $i = 1, 2$ , respectively, are

$$m_i \left[ \ddot{x}_i + \frac{2}{\tau_i} \dot{x}_i + \omega_i^2 (x_i - x_{i0}) \right] = F_i(t), \quad (2.5)$$

where  $x_{i0}$  is the initial position of the mirror such that the separation between the mirrors before switching on the laser is  $L_0 = x_{20} - x_{10}$ . The full system of equations to be evolved in time are the equations from (1) to (5) (non-linearly coupled equations). In section III, we first carry out the task numerically and in later sections, after we have gained sufficient physical insight into the problem, we shall present the semi-analytical results.

### III. THE NUMERICAL SOLUTION

For the numerical calculation, we consider the VIRGO parameters for the suspension and the optical cavity. We assume  $m_1 = m_2 = m \simeq 28$  kg.,  $\omega_1 = \omega_2 = \omega \simeq 3.75$  rad./sec. which corresponds to a resonant frequency of about 0.6 Hz. The  $Q$  factor for the suspension is typically of the order of  $10^6$ . The optical parameters are  $\tau \simeq 2 \times 10^{-5}$  sec., the wavelength of the carrier wave  $\lambda \simeq 1.064 \mu\text{m}$ ,  $r_1 \simeq 0.94$ ,  $r_2 \simeq 1$ . The wave number is  $k = 2\pi/\lambda$  and  $R \simeq 0.94$ . We examine the behaviour of the system with the input power varying between 1 kW to 30 kW. Initial detectors will be operated at input powers  $\sim 1$  kW and advanced detectors at powers of few hundred kW or even upto a MW. Note that these are the input powers for the main cavities after power recycling has been implemented.

With the above values for the parameters, we find that the instabilities set in, on the time-scales of few seconds to few hundred seconds. Since the  $Q$ -factor of the pendulum suspension is so large, the damping in the oscillations can be neglected for the numerical integrations carried over the time intervals  $\ll \frac{Q}{\omega} \sim 10^6$  seconds. Most of our numerical integrations range from few seconds to at most few thousands of seconds. Neglecting damping, the equations of motion for the mirrors become,

$$\ddot{x}_i + \omega^2 (x_i - x_{i0}) = \frac{F_i(t)}{m} = f_i(t), \quad i = 1, 2. \quad (3.1)$$

The equations of motion of the mirrors are non-linear differential equations and cannot be solved by simple methods. We integrate the equations by the so called ‘Phase Space method’ described below:

Let  $\Delta$  be the time-step of integration. The natural time step we assume is  $\Delta = \tau$ . We assume that the forcing term is a constant during each time step. This assumption is not unrealistic because the round trip time interval for the VIRGO cavity is of the order of  $10^{-5}$  seconds; note that this approximation will hold *a fortiori* for more common (much shorter) cavities. The equations simplify enormously under this assumption. Thus we can integrate the equations exactly within this time interval.

The evolution of the equations goes as follows:

$$x_{n+1} = x_n \cos \omega \Delta + p_n \sin \omega \Delta + \frac{f_n(1 - \cos \omega \Delta)}{\omega^2}, \quad (3.2)$$

$$p_{n+1} = -x_n \sin \omega \Delta + p_n \cos \omega \Delta + \frac{f_n \sin \omega \Delta}{\omega^2}, \quad (3.3)$$

where we have dropped the indices 1,2 for simplicity and  $p = \dot{x}/\omega$ . Here,  $x$  represents the displacement from the mean position  $x_0$ . The index  $n$  represents the value of the variable at the time  $n\Delta$ , i.e. for example,  $x_n = x(n\Delta)$ . The optical component has the following iterative evolution:

$$f_{1n} = -\frac{2[R^2 P_{n-1} - r_1^2 P_0]}{mc}, \quad (3.4)$$

$$f_{2n} = \frac{2r_2^2 P_{n-1}}{mc}, \quad (3.5)$$

$$P_n = |B_n|^2, \quad (3.6)$$

$$B_n = t_1 A \exp(ikx_{1n}) + R B_{n-1} \exp(ikL_n), \quad (3.7)$$

$$L_n = 2x_{2n} - x_{1n} - x_{1,n-1}. \quad (3.8)$$

This scheme solves the system of equations. Since it is the length of the cavity that actually matters for this problem, we define the variable,

$$\psi(t) = k[x_2(t) - x_1(t)] - kL_0, \quad (3.9)$$

and present the results in phase space plots of  $\dot{\psi}/\omega$  vs  $\psi$ .  $\psi(t)$  is called the differential mode.

We first consider the case when the mirrors are hanging in the resonance position and the laser is switched on. As the power builds up, the radiation pressure acts on the mirrors, driving them apart resulting in the detuning of the cavity. This reduces the radiation pressure force and the mirrors swing back. The motion is oscillatory and as we note, the oscillations increase in amplitude. We employ two values of input power namely, 1 kW (initial VIRGO) and 30 kW corresponding to advanced detectors. The results are presented by the phase space trajectories of the mirrors. We consider four variables for the purpose,  $x_1$ ,  $x_2$ ,  $\psi$  and  $\phi$ .  $\phi$ , defined later in the text in eq. (24), section IV - B, is called the common mode. For the range of powers considered 1 kW to 30 kW, the phase space curves obtained from numerical simulations, for few tens of seconds are qualitatively the same.

We make the following general observations about the features:

1. We observe from figs.4 and 5 that the radius of the phase space curve increases with every cycle which indicates that the mirrors continuously gain energy from the input laser beam implying that the system is nonconservative. We also observe that the gain per cycle is not constant but some sort of a periodic function of the radius of the phase space diagram. We shall consider this phenomenon in detail in section V.
2. The (static) radiation pressure force peaks when the cavity is in resonance and drops down to zero when it is out of resonance, (see fig.3). The full width at half maximum (FWHM) of the radiation pressure force  $F(\psi)$  is about 0.06 rad, corresponding to the FWHM of the cavity resonance curve for a finesse of 50. Hence, for the initial stretch of the phase space trajectory, the mirrors experience the radiation pressure force whereas during the rest of the time, they only experience the restoring force (and the force due to the input power for  $M1$ ). The phase-space trajectory is circular during the restoring force regime and is deformed away from the circularity when the mirrors encounter the appreciable amount of radiation pressure near resonance (see fig.4).
3. Since the laser is beamed in the positive  $x$ -direction, there is an asymmetry about the origin. This shifts the centre of mass trajectory to the positive side of the  $x$  axis (see fig.4). The period of oscillation of the common mode is twice that of the period of the differential mode of the system (see fig.2).

4. If we let the laser beam pump in energy for large amounts of time, the amplitude also becomes large and the mirrors sweep across several resonances. The phase space trajectory then tends to become more and more circular and the motion approximates to that of a simple harmonic motion. This feature can be observed in all the four modes. The circularity of the trajectory implies that the motion is almost ‘free’. The radiation pressure force has little effect because the mirrors sweep too quickly across the resonances for it to affect their motion. However, as we shall see that the steady gain in energy still persists. Figure 5 depicts this phenomenon.
5. The amount of energy imparted to mirror 2 by the laser beam after getting reflected, is more than to mirror 1. Thus M2 swings with larger amplitude as compared to M1 (see fig.4) (the radiation force is larger on M2).
6. Let’s turn now to the dynamics of a short cavity. The fig.6 shows the space of phase trajectory for the differential mode  $\psi$ , for a short cavity of length  $L_0 = 30$  cm (instead of 3 km for the other examples) and with the same optical and mechanical parameters and initial conditions as in fig.5 obtained with the 3 km long cavity. The round-trip time is here  $\tau \simeq 2 \times 10^{-9}$  s, and the simulation lasts for 500 s (corresponding to a huge number of round trips in the cavity). At the contrary of the kilometric cavity, see fig.5, no energy gain is found. This is in accord with the results of Meystre et al., who have previously developed a theory of radiation-pressure driven cavities [12]. The physical reason for this difference of behaviour between a short (common) cavity and a kilometric one is precisely due to the difference of length, as explained in the following sections. Time delay effects are thus of utmost importance for very long cavities, while they can be neglected for usual ones (and so have been neglected in Meystre’s theory [12]).

#### IV. PHASE SPACE TRAJECTORIES FOR THE FIRST CYCLE

In this section, we obtain approximate closed form expressions for the equations of the phase space trajectories for about a period of one cycle. For the VIRGO case, this turns out to be between one or two seconds. This analysis could be useful in the context of the initial locking of the cavity.

##### A. The differential mode $\psi$

The equations of motion of the individual mirrors, equations (3) to (5) allow us to write the equation of motion of the system of mirrors in the differential mode as,

$$\ddot{\psi} + \omega^2 \psi = \frac{k}{m} [F_2(t) - F_1(t)]. \quad (4.1)$$

In the quasi-static approximation,

$$P(t - \tau) \simeq P(t) = \frac{P_{max}}{1 + \left(\frac{2\mathcal{F}}{\pi}\right)^2 \sin^2 \psi}, \quad (4.2)$$

where  $\mathcal{F} = \pi\sqrt{\mathcal{R}}/(1 - R)$  is the finesse of the cavity and

$$P_{max} = \frac{t_1^2 P_0}{(1 - R)^2}. \quad (4.3)$$

Thus the equation for  $\psi$  is,

$$\frac{\ddot{\psi}}{\omega^2} + (\psi + \psi_0) = \frac{F_0}{1 + \left(\frac{2\mathcal{F}}{\pi}\right)^2 \sin^2 \psi}, \quad (4.4)$$

where

$$F_0 = \frac{2k(r_2^2 + R^2)}{m\omega^2 c} P_{max}, \quad (4.5)$$

and

$$\psi_0 = \frac{2kP_0 r_1^2}{m\omega^2 c}. \quad (4.6)$$

For the VIRGO cavity, we have the following numerical values for the quantities:

$\psi_0 \simeq 0.88P_0/10kW$ ,  $\mathcal{F} \simeq 50$  and  $F_0 \simeq 62.6P_0/10kW$ .

For  $\mathcal{F} \gg 1$ , the term on the right hand side of equation (18) is non-zero only when  $\psi \ll 1$ . With the approximation  $\sin \psi \sim \psi$ , we can easily integrate equation (18) to get the phase space trajectory of the mirrors,

$$\frac{\dot{\psi}^2}{\omega^2} + (\psi + \psi_0)^2 = \frac{F_0\pi}{\mathcal{F}} \tan^{-1}\left(\frac{2\mathcal{F}}{\pi}\psi\right) + \psi_0^2. \quad (4.7)$$

For low powers like 1 kW, the approximation  $\sin \psi \sim \psi$  works remarkably well and agrees with the numerically obtained phase space trajectory. In order to compare the analytical and numerical results, we compare the maximum value of  $\psi$ , namely  $\psi_{max}$ , of the trajectories for various input powers in fig.7.

1. When  $\psi$  is small that is near resonance, the equation of the trajectory reduces to

$$\frac{\dot{\psi}^2}{\omega^2} = 2F_0\psi. \quad (4.8)$$

Thus the trajectory is parabolic in shape and passes through the origin.

2. When  $\psi \sim 1$ , the trajectory is a circle as expected since there is hardly any radiation pressure force acting on the mirrors. The equation of the trajectory in this regime is

$$\frac{\dot{\psi}^2}{\omega^2} + (\psi + \psi_0)^2 = \frac{F_0\pi^2}{2\mathcal{F}} + \psi_0^2. \quad (4.9)$$

When the input power is very large  $\sim 50$  kW, the trajectory does not maintain this simple shape. For example, when  $P_0 = 50$  kW, the trajectory is as shown in fig.8.

This is because the high powers make the mirrors cross several resonances in the first cycle itself and consequently the trajectory has more complex behaviour. We do not pursue this case here.

## B. The common mode $\phi$

In this sub-section, we study the motion of the center of mass of the system of two mirrors. We define the center of mass coordinate of the two mirrors as,

$$\phi = k(x_1 - x_{10}) + k(x_2 - x_{20}). \quad (4.10)$$

The equation of motion of the system in the center of mass coordinate is,

$$\ddot{\phi} + \omega^2\phi = \frac{k}{m}[F_1(t) + F_2(t)], \quad (4.11)$$

where for  $F_1(t)$  and  $F_2(t)$  are given by equations (3) and (4). The equation of motion takes the form,

$$\frac{\ddot{\phi}}{\omega^2} + (\phi - \psi_0) = \frac{F_c}{1 + \left(\frac{2\mathcal{F}}{\pi}\right)^2 \sin^2 \psi}, \quad (4.12)$$

where

$$F_c = \frac{2k(r_2^2 - R^2)t_1^2 P_0}{mc\omega^2(1 - R)^2}. \quad (4.13)$$

For VIRGO parameters,  $F_c \simeq 4.0 \frac{P_0}{10kW}$ . The above equation is a second order differential equation and is coupled nontrivially to the  $\psi$  mode. The strategy we adopt is to study the motion of the center of mass in different regimes; (1) near the resonance and (2) away from the resonance. The full trajectory is obtained by matching the solution in the region of the overlap.

1. For  $0 \leq \psi \leq 0.5$ ;  $\sin \psi \sim \psi$ , equation (26) becomes

$$\frac{\ddot{\phi}}{\omega^2} + (\phi - \psi_0) = \frac{F_c}{1 + (\frac{2\mathcal{F}\psi}{\pi})^2}. \quad (4.14)$$

Further for  $\psi \leq 3 \times 10^{-3}$ ,  $(\frac{2\mathcal{F}\psi}{\pi})^2 \ll 1$ ; we neglect  $(\frac{2\mathcal{F}\psi}{\pi})^2$  as compared to 1 and obtain,

$$\frac{\dot{\phi}^2}{\omega^2} + \phi^2 = 2(F_c + \psi_0)\phi. \quad (4.15)$$

For the VIRGO cavity and input power 1 kW,  $F_c \sim 0.4$ . Neglecting the quadratic term in  $\phi$  as compared to the linear term, we see that the motion of the center of mass describes a parabola for low values of  $\psi$  and  $\phi$ ,

$$\frac{\dot{\phi}^2}{\omega^2} \simeq 0.97\phi. \quad (4.16)$$

We compare the slopes of the phase space diagrams in the differential mode as well as the common mode. The phase space curve is more steeper in the common mode as compared to the differential mode.

2. Away from resonance,  $\psi \geq 0.5$ , the power stored inside the cavity is almost zero. The equation of motion of the center of mass is given by,

$$\ddot{\phi} + \phi = \psi_0. \quad (4.17)$$

The solution for the initial conditions  $\phi = \phi_0, \dot{\phi} = \dot{\phi}_0$  is,

$$\frac{\dot{\phi}^2}{\omega^2} + (\phi - \psi_0)^2 = \frac{\dot{\phi}_0^2}{\omega^2} + (\phi_0 - \psi_0)^2. \quad (4.18)$$

This solution must be matched to the solution in case 1. Suppose we match the solution at  $\phi_0 = 0.5$ , from equation (29) we have  $\dot{\phi}/\omega \sim 0.7$ . This gives the approximate solution. In general, the solution in this region is,

$$\frac{\dot{\phi}^2}{\omega^2} + (\phi - \psi_0)^2 = 2(F_c + \psi_0)\phi_0 + (\phi_0 - \psi_0)^2 - \phi_0^2. \quad (4.19)$$

The equations (29) and (33) describe the full solution for this mode.

The phase space trajectory for the individual mirrors can be obtained from the motion of the mirrors in the differential and the common modes. The trajectories of the  $x_1$  and  $x_2$  modes are shown in figures 2 and 4.

## V. ENERGY CONSIDERATIONS AND ANTI-DAMPING

In the previous section, we examined the motion of the mirrors under the radiation pressure force. We noted that each time when the mirrors cross a resonance they experience an impulsive force. In this section, we analyze in detail as to how the system gains energy as each resonance is encountered.

### A. Quasi-static approximation

We start with the quasi-static approximation in which the system is conservative, thus there is no net gain in energy. We then phenomenologically introduce the ‘time delay’,  $\tau_{lag}$  which now leads to gain in energy. We thus obtain  $\tau_{lag}$  in terms of the cavity parameters and this gives us an equation for an anti-damped harmonic oscillator. The energy gain can be obtained as shown in the following sections. Finally, for large times, the gain can be expressed through a negative  $Q$  of a harmonic oscillator. In the quasi-static approximation, we assume that the mirrors are moving ‘slowly’ that is the intra-cavity power has time to adjust itself to the slowly changing positions of mirrors, i.e.  $\tau\psi \ll 1 - R$ . Thus neglecting  $\tau$  from the equation of motion we obtain,

$$\frac{\ddot{\psi}}{\omega^2} + (\psi + \psi_0) = F_s(\psi), \quad (5.1)$$

where  $\psi_0$  as given in the previous section gives the constant displacement due to the constant input power  $P_0$  from the laser beam and  $F_s(\psi)$  is the radiation pressure force in the static case is given by,

$$F_s(\psi) = \frac{F_0}{1 + (\frac{2F}{\pi})^2 \sin^2 \psi}, \quad (5.2)$$

where  $F_0$  is given in equation (19). The dimensionless energy of the system is an integral of motion and is obtained as

$$E = \frac{1}{2} \dot{\psi}^2 + V_{sus}(\psi) + V_0(\psi) + V_{rad}(\psi), \quad (5.3)$$

where the potentials are given by,

$$V_{sus}(\psi) = \frac{1}{2} \psi^2, \quad (5.4)$$

$$V_0(\psi) = \psi_0 \psi, \quad (5.5)$$

$$V_{rad}(\psi) = - \int_0^\psi F_s(\psi) d\psi. \quad (5.6)$$

The system is conservative in this approximation. These results have been obtained in the earlier literature [14].

However, we note from the results of numerical simulations that the system indeed gains energy with every cycle of oscillation. Moreover, this gain occurs when the radiation pressure force is appreciable i.e. when the system is near resonance. Most importantly, we observe from the numerical simulations that radiation pressure force lags behind its quasi-static value by a ‘time-lag’ which we denote by  $\tau_{lag}$ . We find that in the case of VIRGO,  $\tau_{lag}$  varies from about  $16\tau$  to  $30\tau$  as one climbs up the resonance curve from half its maximum to the maximum.  $\tau_{lag}$  is of the order of the storage time of the cavity. With this in mind we write the force  $F(t) \sim F_s(t - \tau_{lag})$  and obtain the following equation of motion,

$$\frac{\ddot{\psi}}{\omega^2} + (\psi + \psi_0) = F_s(\psi(t - \tau_{lag})). \quad (5.7)$$

Taylor expanding the forcing term to the first order we obtain,

$$\frac{\ddot{\psi}}{\omega^2} + \tau_{lag} \frac{dF_s}{d\psi} \dot{\psi} + (\psi + \psi_0) = F_s(\psi), \quad (5.8)$$

as the equation of motion for the system. The  $\dot{\psi}$  term in equation (41) is responsible to the gain/loss of energy of the system. This solely depends on the sign of  $\frac{dF_s}{d\psi}$  since  $\tau_{lag}$  is always positive. If we start the system from resonance at  $\psi = 0$ ,  $\psi$  starts increasing slowly and in the region,  $\frac{dF_s}{d\psi} < 0$  and the system experiences more force than what it would have been in the quasi-static case. This excess force is manifested in an excess amount of energy  $\Delta E$ . In general, the energy gained/lost over a certain amount of time is given by,

$$\Delta E = - \int_{\psi_1}^{\psi_2} \tau_{lag}(\psi) \frac{dF_s}{d\psi} \dot{\psi} d\psi = - \int_{t_1}^{t_2} \tau_{lag} \frac{dF_s}{d\psi} \dot{\psi}^2 dt. \quad (5.9)$$

It is clear from equation (42) that when  $\frac{dF_s}{d\psi} < 0$ , the energy gain  $\Delta E > 0$  and vice-versa. But since the radiation pressure force always gives a kick in the positive  $-\psi$  direction, the  $|\dot{\psi}|$  is always larger when  $\frac{dF_s}{d\psi} < 0$ . In other words, the amount of energy gained by the system is more than the amount of energy lost. Hence, there is always a net gain in energy when the system crosses a resonance. We need to compute this extra force  $\Delta F$  which gives rise to the gain in the energy to the first order in  $\tau_{lag}$ . We obtain,

$$\Delta F = - \frac{dF_s}{d\psi} \dot{\psi} \tau_{lag}. \quad (5.10)$$



We note that  $\Delta F$  depends on the phase velocity and  $\frac{dF_s}{d\psi}$ . Since  $\frac{dF_s}{d\psi} \simeq 0$  when the system is away from resonance,  $\Delta F$  comes into play only in the region of resonance. Another way of describing the fundamental asymmetry is to say that for the moving mirror, the wavelength of the laser light is modified by the Doppler effect. When the mirrors are approaching each other, the apparent frequency of the light for the cavity is increased, or equivalently, the line-width of the cavity seen from the laboratory frame is narrower and vice versa when the mirrors move away from one another, the line-width is seen to be broader. The consequence is that the braking force (when the mirrors move against the light) acts for a shorter time than the accelerating force, when the mirrors are moving away from each other. Over one cycle the energy difference is positive and there is a continuous increase of mechanical energy which comes from the laser.

## B. The computation of the time-delay

In this section, we obtain a closed form expression for the ‘time-delay’,  $\tau_{lag}$  under the approximation that the relative velocity of the mirrors does not change much during the storage time of the cavity. This is observed in the numerical simulations and hence the approximation may be justified.  $\tau_{lag}$  is the most important quantity for computing the rate of gain in energy. The intra-cavity radiation field at  $n$ -th time instant  $B_n$  is related to the intra-cavity field at  $n+1$ -th time instant via an iterative relation,

$$B_{n+1} = t_1 A + R \exp(2i\psi_n) B_n, \quad (5.11)$$

where,  $B_n = B(n\tau)$ ,  $\psi_n = \psi(n\tau)$ . We compute the field  $B_n$  from initial time  $t_0$ , which we take to be zero. We take the time step for the iteration to be the round trip time  $\tau$ . In order to compute the intra-cavity field, it is necessary to know the temporal behaviour of  $\psi$ . For the static case, when the mirrors are stationary, we get the equilibrium field  $B_s$ . When the mirrors are moving, the approximation now comes into play, namely, we assume that  $\dot{\psi}$  is constant over the storage time of the cavity.

The Taylor expansion of  $\psi_k$  to the first order around  $t = 0$  is,

$$\psi_k = \psi_0 + k\tau\dot{\psi}_0, \quad (5.12)$$

where  $\psi_0 = \psi(t = 0)$ . Iterating equation (44)  $n$  times starting from  $t = 0$  when  $B = B_0$ , we obtain,

$$B_n = t_1 A \sum_{m=0}^{n-1} R^m e^{2i \sum_{k=n-m}^{n-1} \psi_k} + R^n e^{2i \sum_{k=0}^{n-1} \psi_k} B_0. \quad (5.13)$$

For large  $n$ , the last term in equation (46) tends to zero and the electric field amplitude at the  $n$ -th iteration is given by,

$$B_n = t_1 A \sum_{m=0}^{n-1} R^m e^{2i \sum_{k=n-m}^{n-1} \psi_k}. \quad (5.14)$$

- If the relative separation between the mirrors is constant in time,  $\psi_k = \psi_0$ , we retrieve the equilibrium field  $B_s$ :

$$B_s = t_1 A \sum_{m=0}^{\infty} R^m e^{2im\psi_0} = \frac{t_1 A}{1 - R e^{2i\psi_0}}. \quad (5.15)$$

- Turning now to the case in hand, when  $\psi_k$  varies linearly with time, the sum in the exponential for large  $n$  is approximately given by

$$\sum_{k=n-m}^{n-1} \psi_k \sim m\psi_n - \frac{1}{2} m^2 \tau \dot{\psi}_0. \quad (5.16)$$

We combine equations (47) and (49) to obtain,

$$B_n = t_1 A \sum_{m=0}^{n-1} R^m e^{2im\psi_n} e^{-im^2 \tau \dot{\psi}_0}. \quad (5.17)$$

If  $\dot{\psi}$  is small then the exponent can be linearized. Then it is possible to express the field as the sum of the static term  $B_s$  and the remaining part  $\Delta B$  which corresponds to the time lag. We write

$$B_n = B_s + \Delta B, \quad (5.18)$$

where

$$\Delta B = -i\tau t_1 A \dot{\psi}_0 \sum_{m=0}^{n-1} R^m e^{2im\psi_n} m^2. \quad (5.19)$$

Summing the arithmetico-geometric series [17] yields,

$$\Delta B = -2it_1 A \tau \frac{\dot{\psi} R^2 e^{-4i\psi}}{(1 - R e^{-2i\psi})^3}. \quad (5.20)$$

The corresponding power  $\Delta P$  is given by

$$\Delta P = 2Re(B_n \Delta B_n^*) \sim \frac{16t_1^2 |A|^2 \tau R^2 \dot{\psi} \psi (1 - R)}{[(1 - R)^2 + 4R\psi^2]^3}. \quad (5.21)$$

Referring to equation (19), we get the expression for the dimensionless extra force,

$$\Delta F = \frac{2k(r_2^2 + R^2)}{m\omega^2 c} \Delta P. \quad (5.22)$$

The above expression of power is for values of  $\psi$  near resonance when  $\psi \ll 1$ . When  $\psi \sim n\pi$ , the same expression can be replaced by the  $\psi - n\pi$  under similar approximations. The effective ‘time delay’  $\tau_{lag}$  is now obtained from (43), (54) and (55).

$$\tau_{lag} = \frac{2\tau R}{(1 - R)(1 + (\frac{2\mathcal{F}}{\pi})^2 \psi^2)}. \quad (5.23)$$

We note from the equation (56) that the effective time lag is maximum at the resonance and starts decreasing as one goes away from the resonance value. For VIRGO parameters, we compute the value of the  $\tau_{lag}$ . At FWHM, i.e.  $\psi \sim 0.03$ ,  $\tau_{lag} \sim 16\tau$ , going up to  $\tau_{lag} \sim 30\tau$  as one approaches resonance.

### C. Energy gain near the resonance at $\psi = 0$

In this section, we examine the motion of the mirrors for small amplitudes. Initially before the laser is switched on, the cavity is at resonance i.e. the two mirrors are separated by an integral multiple of  $\pi$  in phase ( $\frac{kL_0}{\pi}$  is an integer). The system starts from  $\psi = 0$  and the motion is allowed to evolve with time. We restrict the amplitude to  $|\psi| \leq \pi$  and study the system in this regime. Our goal is to compute the net gain in energy,  $\Delta E_{cycle}$  during one cycle of oscillation. We have,

$$\Delta E_{cycle} = 2 \int_0^{\psi_1} \Delta F(\psi) d\psi, \quad (5.24)$$

where

$$\Delta F(\psi) = \frac{16\tau R^2 F_0 \dot{\psi} \psi}{(1 - R)^3 (1 + (\frac{2\mathcal{F}\psi}{\pi})^2)^3}. \quad (5.25)$$

We note that  $\frac{dF_s}{d\psi} \leq 0$  in this regime. We set an arbitrary cut-off  $\psi_1$  (when  $\Delta F \ll 1$ ) as the system moves away from the resonance. The factor of two is because the force is encountered twice during the cycle. The  $\dot{\psi}$  is obtained from the energy balance equation,

$$\frac{1}{2} \frac{\dot{\psi}^2}{\omega^2} = \int_0^\psi F_s(\psi) d\psi \sim \frac{\pi}{2\mathcal{F}} F_0 \tan^{-1}\left(\frac{2\mathcal{F}\psi}{\pi}\right). \quad (5.26)$$

Thus from (57) and (58) we get,

$$\Delta E_{cycle} = 8\omega\tau \sqrt{\frac{R\mathcal{F}}{\pi}} F_0^{3/2} I(\phi_1), \quad (5.27)$$

where,

$$I(\phi_1) = \int_0^{\phi_1} \frac{\phi(\tan^{-1}\phi)^{1/2}}{(1+\phi^2)^3} d\phi, \quad (5.28)$$

and  $\phi_1 = 2\mathcal{F}\psi_1/\pi$ . The cut-off  $\phi_1$  should be away from the resonance and we find for VIRGO,  $\phi_1 \sim 5$  is an acceptable value.

The numerical and the analytical results are compared in fig.9 by plotting the gain in energy per cycle for various input powers.

#### D. Energy gain for large amplitudes

As the mirrors gain energy, they swing with ever increasing amplitude and sweep over several resonance peaks of the Fabry-Perot cavity. The system gains energy at every resonance peak and thus the energy gained per cycle is the sum of the energy gained at each resonance encountered. The peaks are encountered at  $\psi = n\pi$ , with  $n_{max} \geq n \geq n_{min}$ ,  $n_{min} < 0$  and  $n_{max} > 0$ . The total number of resonances encountered by the mirrors is  $n_{max} + |n_{min}| + 1$ . Also it is observed that  $n_{max} \geq |n_{min}|$  due to the built-in asymmetry arising due the laser power pumped in the positive  $x$ -direction (see fig.3).

Let  $\Delta E_n$  be the energy gain at the  $n$ -th resonance, then the total energy gained per cycle  $\Delta E_{cycle}$  is given by,

$$\Delta E_{cycle} = \sum_{n_{min}}^{n_{max}} \Delta E_n, \quad (5.29)$$

where

$$\Delta E_n = \Delta E_{n+} + \Delta E_{n-}, \quad (5.30)$$

and  $\Delta E_{n-}$ ,  $\Delta E_{n+}$  is the energy lost or gained respectively and given by the following expressions,

$$\Delta E_{n+} = \int_{n\pi}^{n\pi+\psi_1} \Delta F d\psi > 0, \quad (5.31)$$

$$\Delta E_{n-} = \int_{n\pi-\psi_1}^{n\pi} \Delta F d\psi < 0. \quad (5.32)$$

Combining equations (57,58,62 to 65) we get the energy gain at  $n\pi$  as,

$$\Delta E_n \simeq \frac{16\tau R^2 F_0}{(1-R)^3} (\dot{\psi}_{n+} - \dot{\psi}_{n-}) \int_0^{\psi_1} \frac{\psi}{(1 + (\frac{2\mathcal{F}\psi}{\pi})^2)^3} d\psi, \quad (5.33)$$

where  $\dot{\psi}_{n-}$  and  $\dot{\psi}_{n+}$  are the relative phase velocities of the mirrors for  $\psi \leq n\pi$  and  $\psi \geq n\pi$  respectively. The energy gained at different resonance positions of the mirrors is different because the  $\psi$  is different at different resonances,  $\psi$  is maximum when  $|n|$  is small and becomes small when  $n$  approaches  $n_{min}$  or  $n_{max}$ . Thus the net energy gain per cycle is

$$\Delta E_{cycle} \simeq \frac{\tau R^2 F_0}{(1-R)^3} \left(\frac{\pi}{\mathcal{F}}\right)^2 \sum_{n_{min}}^{n_{max}} (\dot{\psi}_{n+} - \dot{\psi}_{n-}). \quad (5.34)$$

The next task is to compute the  $(\dot{\psi}_{n+} - \dot{\psi}_{n-})$ , the increase in phase space velocity while crossing the resonance position as a function of  $n$ . For large values of  $n$ , the radiation pressure effect reduces remarkably as is observed in fig.3. Hence we take the static force equation to compute the increase in the phase space velocities. We integrate equation (41) neglecting the anti-damping term obtaining the change in kinetic energy as,

$$\frac{1}{2\omega^2}(\dot{\psi}_{n+}^2 - \dot{\psi}_{n-}^2) = F_0 \int_{-\infty}^{\infty} \frac{1}{1 + (\frac{2\mathcal{F}}{\pi})^2 \psi^2} d\psi - 2\psi_1\psi_0 - 2n\pi\psi_1. \quad (5.35)$$

Equation (68) reduces to

$$\frac{(\dot{\psi}_{n+} - \dot{\psi}_{n-})}{\omega} = \frac{\frac{\pi^2 F_0}{\mathcal{F}} - 4\psi_1(\psi_0 + n\pi)}{2\dot{\psi}(n\pi)/\omega}, \quad (5.36)$$

where we have approximated  $\dot{\psi}_{n+} + \dot{\psi}_{n-} \simeq 2\dot{\psi}(n\pi)$ .

To compute  $\dot{\psi}(n\pi)/\omega$  analytically, we consider the dimensionless instantaneous energy as given by equation (36),

$$E = \frac{1}{2} \frac{\dot{\psi}^2}{\omega^2} + \frac{1}{2}(\psi^2 + 2\psi\psi_0) - \frac{2k(r_2^2 + R^2)t_1^2 P_0}{m\omega^2 c} J(\psi), \quad (5.37)$$

where  $J(\psi) = \int_0^\psi \frac{d\psi}{(1-R)^2 + 4R \sin^2 \psi}$ . We can approximate the integral for large motions as  $J(\psi) \sim \frac{n\pi}{1-R^2} \sim \frac{\psi}{1-R^2}$  for  $n$  crossings of the resonances. Assuming  $r_2 = 1$  and  $r_1 = R$ , we have,

$$\frac{\dot{\psi}^2}{\omega^2} + (\psi - \psi_c)^2 = (2E + \psi_c^2), \quad (5.38)$$

where  $\psi_c = \frac{2kF_0}{m\omega^2 c} \sim \frac{P_0}{10kW}$  (for VIRGO parameters). The phase space trajectory is a circle centred around  $\psi_c$  with radius

$$\rho = \sqrt{2E + \psi_c^2}. \quad (5.39)$$

Equation (71) gives  $\frac{\dot{\psi}(n\pi)}{\omega}$  as

$$\frac{\dot{\psi}(n\pi)}{\omega} = \sqrt{\rho^2 - (n\pi - \psi_c)^2}. \quad (5.40)$$

We rewrite the gain in energy per cycle as,

$$\Delta E_{cycle} = \frac{\tau R^2 F_0 \omega}{(1-R)^3} \left(\frac{\pi}{\mathcal{F}}\right)^2 S(n_{max}, n_{min}), \quad (5.41)$$

where  $n_{max}$  is the greatest integer not greater than  $(\psi_c + \rho)/\pi$  and  $n_{min}$  is the smallest integer not smaller than  $(\psi_c - \rho)/\pi$ . We have,

$$S(n_{max}, n_{min}) = \sum_{n=n_{min}}^{n_{max}} g(n\pi), \quad (5.42)$$

where

$$g(n\pi) = \frac{\frac{\pi^2 F_0}{2\mathcal{F}} - 2\psi_1(\psi_0 + n\pi)}{\sqrt{\rho^2 - (n\pi - \psi_c)^2}}. \quad (5.43)$$

For large motion of the mirrors, since the mirrors cross many resonances, we may replace the sum by an integral over  $n$ . Changing over to the variable  $M = n\pi - \psi_c$ , in which the system appears more symmetric about the origin, we have,

$$S = \int_{M_{min}}^{M_{max}} \frac{\alpha - \beta M}{(\rho^2 - M^2)^{1/2}} dM \quad (5.44)$$

where  $\alpha = \frac{\pi F_0}{2\mathcal{F}} - \frac{2\psi_1}{\pi}(\psi_0 + \psi_c)$  and  $\beta = \frac{2\psi_1}{\pi}$ .  $M_{max}$  and  $M_{min}$  correspond to  $n_{max}$  and  $n_{min}$  respectively. We note that  $\rho$  satisfies the following inequalities,

$$M_{max} \leq \rho \leq M_{max} + 1, \quad |M_{min}| \leq \rho \leq |M_{min}| + 1. \quad (5.45)$$

We observe that when  $n$  is large, the difference between  $|M_{min}|$  and  $M_{max}$  is small, of the order of 1 or 2 times  $\pi$ . We denote the difference, by  $\delta M$  where,

$$\delta M = M_{max} - |M_{min}| = M_{max} + M_{min}. \quad (5.46)$$

The integral in equation (77) splits into three parts  $S = S_1 - S_2 - S_3$ , where

$$S_1 = 2\alpha \sin^{-1} M_{max}/\rho, \quad (5.47)$$

$$S_2 \simeq \delta M \frac{2\alpha}{(\rho^2 - M_{max}^2)^{1/2}}, \quad (5.48)$$

$$S_3 \simeq \beta \frac{M_{max} \delta M}{(\rho^2 - M_{max}^2)^{1/2}}. \quad (5.49)$$

The dominant term is  $S_1$  which gives the general behaviour and shape of the curve shown in fig.10. While  $S_2$  produces a small kink in the curve, the effect of  $S_3$  can essentially be ignored. In case of the VIRGO cavity and  $P_0 = 30$  kW and  $\rho \simeq 20$ ,  $S_1 \simeq 16.7$ ,  $S_2 \simeq 1.75$  and  $S_3 \simeq 0.26$ . For the initial VIRGO detector,  $P_0 = 1$  kW, and  $\rho \simeq 4.0$ ,  $S_1 \simeq 0.56$  while  $S_2, S_3 \simeq 0$ .

Considering only  $S_1$ , the energy gain per cycle is approximately given by,

$$\Delta E_{cycle} = \frac{2\Delta E_{max}}{\pi} \sin^{-1} \frac{M_{max}}{\rho}, \quad M_{max} \leq \rho \leq M_{max} + 1, \quad (5.50)$$

where,

$$\Delta E_{max} = \frac{\tau R^2 F_0 \omega \pi^3}{(1-R)^3 \mathcal{F}^2} \left( \frac{\pi F_0}{2\mathcal{F}} - \frac{2\psi_1}{\pi}(\psi_0 + \psi_c) \right). \quad (5.51)$$

We observe the following features in the profile of  $\Delta E_{cycle}$ :

- At the resonance position,  $\rho = M_{max}$  the energy gain is maximum and equal to  $\Delta E_{max}$ . For the VIRGO cavity specifications and input power of 30 kW,  $\Delta E_{max} \simeq 3.8$ . When  $P_0 = 1$  kW,  $\Delta E_{max} \simeq 4.2 \times 10^{-2}$ .
- Equation (83) shows that the energy gain per cycle is a decreasing function of  $\rho$ . The energy gain decreases till the next resonance is crossed, where it suddenly increases to  $\Delta E_{max}$ . As the amplitude increases,  $\rho$  increases from  $M_{max}$  to  $M_{max} + 1$ , the mirrors sweep across the resonances a little faster which deprives them from gaining the full energy  $\Delta E_{max}$ .  $\Delta E_{cycle}$  therefore reduces from  $\Delta E_{max}$  to  $\Delta E_{min}$ , where

$$\Delta E_{min} = \frac{2\Delta E_{max}}{\pi} \sin^{-1} \frac{M_{max}}{M_{max} + 1}. \quad (5.52)$$

- The energy profile in this range of  $\rho$  i.e.  $M_{max}$  to  $M_{max} + 1$  can be approximately given by,

$$(\Delta E_{max} - \Delta E_{cycle})^2 = \frac{8(\Delta E_{max})^2}{\pi^2 M_{max}} (\rho - M_{max}). \quad (5.53)$$

We note that the minimum value is,

$$\Delta E_{min} \sim \Delta E_{max} \left( 1 - \left( \frac{8}{\pi^2 M_{max}} \right)^{1/2} \right), \quad (5.54)$$

and it tends to the maximum value  $\Delta E_{max}$  as  $M_{max}$  becomes very large.

- In fig.10, it is seen that there is a kink after  $\Delta E_{min}$  is reached. The kink occurs because  $M_{min}$  reduces by 1 when the mirrors cross yet another resonance on the negative side. This is accounted for by the second term.

Since the  $E \sim \rho^2$ , the rate of increase of  $\rho$  per cycle, denoted by  $\Delta \rho$  is given by  $\Delta \rho = \frac{\Delta E}{\rho}$ .

## E. The negative Q-factor

In the previous section, we have seen that for large values of  $\rho$ , the amount of energy gained by the system of two mirrors per cycle is a constant and tends to  $\Delta E_{max}$ . The system is an anti-damped harmonic oscillator which gains on an average, constant amount of energy per cycle. We may therefore associate a *negative* quality factor  $-Q$ , where  $Q > 0$ , with the system which describes the anti-damping. In this section, we endeavor to study the behaviour of  $Q$ . The equation of motion of an anti-damped harmonic oscillator is given by,

$$\frac{\ddot{\chi}}{\omega^2} - \frac{\dot{\chi}}{\omega Q} + \chi = 0, \quad (5.55)$$

where  $Q$  is constant. The solution for  $\chi$  is of the form

$$\chi \sim \chi_0 e^{\omega t/2Q} e^{\pm i\omega t}. \quad (5.56)$$

where  $\chi = \psi - \psi_c$ . The amplitude is  $\rho \sim \chi_0 e^{\omega t/2Q}$  when  $\rho$  is sufficiently large so that the phase space trajectory is approximately circular and can be compared to a simple harmonic oscillator. Since a constant amount of energy is gained per cycle, the  $Q$  will be a function of time. However, we can still describe the system by an average  $Q$  taken over a cycle, which we denote by  $\langle Q \rangle_{cycle}$ , since the change in  $Q$  during one cycle is small. Moreover, we assume  $\frac{1}{\omega \langle Q \rangle_{cycle}} \frac{d\langle Q \rangle_{cycle}}{dt} \ll 1$  i.e. the fractional variation of  $\langle Q \rangle_{cycle}$  over a period of a cycle can be ignored. Thus we obtain a W.K.B. solution for  $\rho(t)$  as,

$$\rho(t) = \rho(t_0) \exp \left[ \frac{1}{2} \int_{t_0}^t \frac{\omega dt}{\langle Q \rangle_{cycle}} \right], \quad (5.57)$$

where  $t_0$  is some fixed but arbitrary initial time instant and  $\rho(t_0)$  is the radius of the circular phase-space trajectory at  $t_0$ . We have also assumed that  $\langle Q \rangle_{cycle} \gg 1$ . From equations (72) and (90) the energy of the harmonic oscillator is given by,

$$E(t) - E(t_0) = \frac{1}{2} \rho^2(t_0) \left[ \exp \left( \int_{t_0}^t \frac{\omega dt}{\langle Q \rangle_{cycle}} \right) - 1 \right]. \quad (5.58)$$

Since the energy gain is a constant and during a cycle equal to  $\Delta E_{max}$ , we can equate  $\frac{2\pi}{\omega} \frac{dE}{dt}$  to  $\Delta E_{max}$  to obtain,

$$E(t) - E(t_0) = \frac{\omega \Delta E_{max}}{2\pi} (t - t_0). \quad (5.59)$$

The time evolution of  $\rho$  is obtained, which yields,

$$\rho(t) = \rho(t_0) \left[ 1 + \frac{\Delta E_{max}}{\pi \rho_0^2} \omega (t - t_0) \right]^{1/2}. \quad (5.60)$$

Equating the logarithmic derivatives of (90) and (93) we obtain,

$$\langle Q \rangle_{cycle}(t) = \langle Q \rangle_{cycle}(t_0) + \omega(t - t_0), \quad (5.61)$$

where  $\langle Q \rangle_{cycle}(t_0) = \frac{\pi \rho^2(t_0)}{\Delta E_{max}}$ . We observe that both the energy and the  $\langle Q \rangle_{cycle}$  increase linearly with time while the amplitude  $\rho$  increases as  $t^{1/2}$ .  $\langle Q \rangle_{cycle}(t)$  depends through  $\Delta E_{max}$  on the input power, finesse and the round trip time.

For  $P_0 = 30$  kW of input power, the trajectory more or less obtains a circular shape when  $\rho(t_0) \sim 15$ . For the VIRGO parameters,

$$\Delta E_{max} \sim 0.42 \left( \frac{P_0}{10 \text{ kW}} \right)^2 \sim 3.79. \quad (5.62)$$

Thus  $\langle Q \rangle_{cycle}(t_0) \sim 186$  and so

$$\langle Q \rangle_{cycle}(t) \sim 186 + \omega(t - t_0). \quad (5.63)$$

Further, if we also consider the effect of the damping of the suspension then the limit cycle will be approached when  $\langle Q \rangle_{cycle} \sim Q_{sus} \sim 10^6$  for VIRGO.  $\langle Q \rangle_{cycle}$  will attain this value after  $\omega t \sim 10^6$  which corresponds to little more than 3 days. The corresponding amplitude is given by,

$$\rho = \rho(t_0) \left[ 1 + \frac{\omega(t - t_0)}{\langle Q \rangle_{cycle}(t_0)} \right]^{1/2} \sim 1100. \quad (5.64)$$

This simple analysis will have to be modified when the limit cycle is almost reached, that is when,  $\langle Q \rangle_{cycle} \sim Q_{sus}$ . Here, however our goal was to estimate the time it takes to reach this stage. The above analysis is then adequate for the purpose. However, when the servo operates or otherwise such a situation is unlikely to arise because other effects such as mirror tilting etc. will be important long before and then the dynamics will be completely different.

## VI. THE EQUILIBRIUM CASE

Lastly, we examine the case when the mirrors are in equilibrium under the radiation pressure force and the restoring force. We have to determine whether the equilibrium is stable or unstable. To this end, we perturb the equation (41) about a given equilibrium point. Writing  $\psi = \psi_{eq} + \delta\psi$  and linearizing, we get,

$$\delta\ddot{\psi} - \frac{2}{\tau_{eq}}\delta\dot{\psi} + \Omega^2\delta\psi = 0, \quad (6.1)$$

where,

$$\tau_{eq} = -\left(\frac{\pi}{2\mathcal{F}}\right)^3 \frac{(1 + (\frac{2\mathcal{F}\psi_{eq}}{\pi})^2)^3}{F_0\psi_{eq}\tau\sqrt{R}}, \quad (6.2)$$

and

$$\Omega_{eq}^2 = 2\left(\frac{2\mathcal{F}}{\pi}\right)^2 \frac{\psi_{eq}F_0}{(1 + (\frac{2\mathcal{F}\psi_{eq}}{\pi})^2)^2}. \quad (6.3)$$

If  $\psi_{eq} \leq 0$ ,  $\Omega_{eq}^2 \leq 0$ , the sign of  $\tau_{eq}$  does not matter and the instability grows exponentially. If on the other hand  $\psi_{eq} > 0$ , then although  $\Omega_{eq}^2 > 0$ ,  $\tau_{eq} > 0$  and this leads to gradually growing oscillations until the pendulum tips over the maximum. We plot the phase space trajectory for the input power of 1 kW in fig.11. We conclude from this that the cavity is *always* unstable when radiation pressure forces act. The time-delay plays a crucial role in making the system unstable. The negative Q-factor for the motion of the mirrors near the equilibrium position, is given by,

$$Q = -\frac{1}{2}\Omega_{eq}\tau_{eq}. \quad (6.4)$$

For an input power of 30 kW, with VIRGO cavity parameters, the equilibrium position of the mirrors near the resonance at zero is  $\psi_{eq} \simeq 0.25$ . The corresponding values of the other quantities are  $\Omega_{eq} \simeq 4.75$  and  $\tau_{eq} \simeq 10^4$  seconds. The negative Q-factor,  $Q \simeq -2.3 \times 10^4$ . Whereas for initial VIRGO,  $P_0 \simeq 1$  kW,  $\psi_{eq} \simeq 0.16$  thus  $\Omega_{eq} \simeq 1.67$ ,  $\tau_{eq} \simeq 3.1 \times 10^4$  seconds, the negative Q-factor,  $Q \simeq -2.6 \times 10^4$ .

## VII. CONCLUSION

We have analysed the effect of radiation pressure on the freely hanging mirrors (no servo loop) suspended in the laser interferometric optical cavities. After numerically evolving the full set of equations of motion with respect to time, we find that the amplitude of the mirror oscillations continuously increases as time progresses. We introduce the ‘time delay’, that is the time taken for field to adjust to the motion of the mirrors, in a phenomenological way to explain the observed gain. We conclude that the gain in energy is due to the differential radiation pressure force arising from the asymmetry depending upon the motion of the mirrors. From another viewpoint, we can also explain the gain in energy qualitatively by the Doppler effect. With respect to the mirror, the frequency of the incoming laser beam is higher as compared to that of the outgoing laser beam due to the Doppler effect. The deficit of the energy of the laser beam after getting reflected from the mirror can be looked upon as the energy gained by the mirrors. The values of the energy gain per cycle are computed analytically under the reasonable assumption that the mirrors are

not accelerated within the time scale of the storage time of the cavity. For VIRGO parameters, the analytical values agree remarkably with the numerical values. The interesting point to note is that the motion of the mirrors approaches that of an anti-damped harmonic oscillator with a constant gain in energy as time progresses which implies that the mirrors move too quickly to get affected by the radiation pressure force. The negative Q-factor of the anti-damped oscillator depends on the input power, the finesse and the round trip time of the cavity and increases linearly as a function of time. The analysis will have to be modified when the negative Q-factor becomes of the order of the damping Q-factor of the suspension fibre, if such a case can arise.

In this paper, we have shown that the radiation pressure force makes the freely hanging mirror unstable *for all values of the input power and irrespective of the initial conditions*.

The above analysis is relevant in the event, when the interferometer is in operation and if the servo loop is suddenly opened. Then the motion of the hanging mirrors can be deduced from the above analysis. This analysis will be helpful in designing a servo-control which can prevent this instability. In a previous work [11], the servo-control was included in the linear regime of the Fabry-Perot curve assuming the transfer function for the servo given by Caron et al. [18]. Their work sets the stage for analysing the system in the non-linear regime as well, but it is then needed to know how servo-control operates in the full regime.

### VIII. ACKNOWLEDGEMENT

The authors thank the IFCPAR (project no. 1010 - 1) under which a substantial part of this work was carried out. One of us (SVD) thanks the PPARC, U.K. for financial support, where this work was finished.

- 
- [1] A.Abramowici et al., Science., 256 (1992).
  - [2] C.Bradaschia et al., Nucl.Instrum. Methods Phys.Res., Sect.**A**, 518 (1990).
  - [3] H. Lück et al., Class. Quantum Grav., **14** 1461 (1997)
  - [4] K. Tsubono et al., in Proceedings of the TAMA Workshop, Edited by K. Tsubono, M.-K. Fujimoto and K. Kuroda, Universal Academy Press, 1997.
  - [5] R.J.Sandeman, in Proceedings of the Second Workshop on Gravitational Wave Data Analysis, Edited by M. Davies and P. Hello, Editions Frontières, 1998.
  - [6] S. V. Dhurandhar, P. Hello, B. S. Satyaprakash and J-Y Vinet, Applied Optics, **36**, 5325 (1997).
  - [7] W. Winkler, K. Danzmann, A. Rudiger and R. Schilling, Phys. Rev. A **44**, 7022 (1991).
  - [8] P. Hello and J-Y. Vinet, J. Phys. (Paris) **51**, 1267 (1990).
  - [9] P. Hello and J.-Y. Vinet, J. Phys. (Paris) **51**, 2243 (1990)
  - [10] P. Hello and J-Y. Vinet, Phys. Lett. A **178**, 351 (1993)
  - [11] V. Chickarmane, S. V. Dhurandhar, R. Barillet, P. Hello and J.-Y. Vinet, Applied Optics, **37**, 3236 (1998).
  - [12] P. Meystre, E.M. Wright, J.D. McCullen and E. Vignes, J.Opt.Soc.Am. B2, 1830 (1985).
  - [13] A. Dorsel, J. D. McCullen, P. Meystre, E. Vignes and H. Walther, Phys. Rev. Lett. **51**, 1550 (1985).
  - [14] N. Deruelle and P. Tourrence, Gravitation, Geometry and Relativistic Physics, (Springer-Verlag, Berlin, 1984).
  - [15] J. M. Aguirregabiria and L. Bel, Phys. Rev. A **36**, 3768 (1987).
  - [16] B. J. Meers and N. McDonald, Phys. Rev.A **40**, 3754 (1989).
  - [17] Gradshteyn-Ryzhik, *Tables of Integrals, Series and Products*, 5th ed., pg.no.1.
  - [18] B. Caron et.al, Astropart. Phys. **6**, 245 (1997).



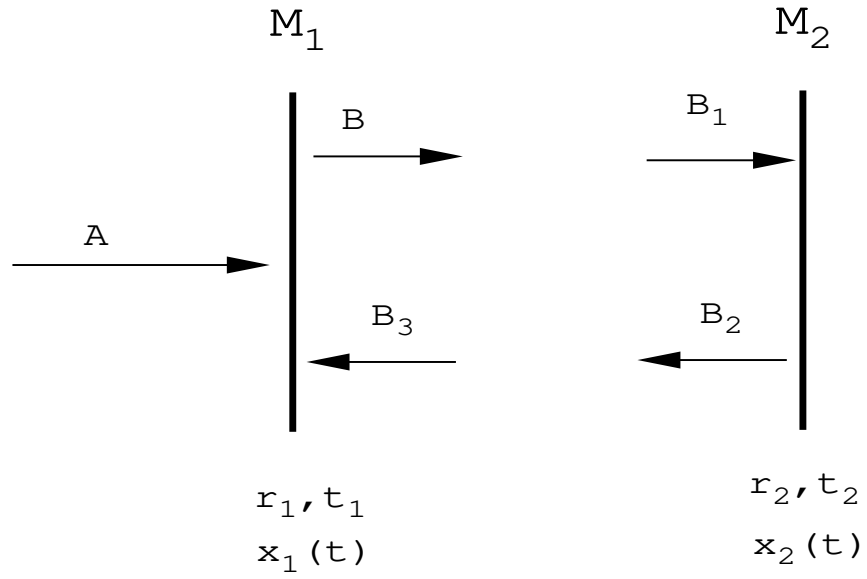


FIG. 1. Schematic diagram of the cavity and the intra-cavity fields.

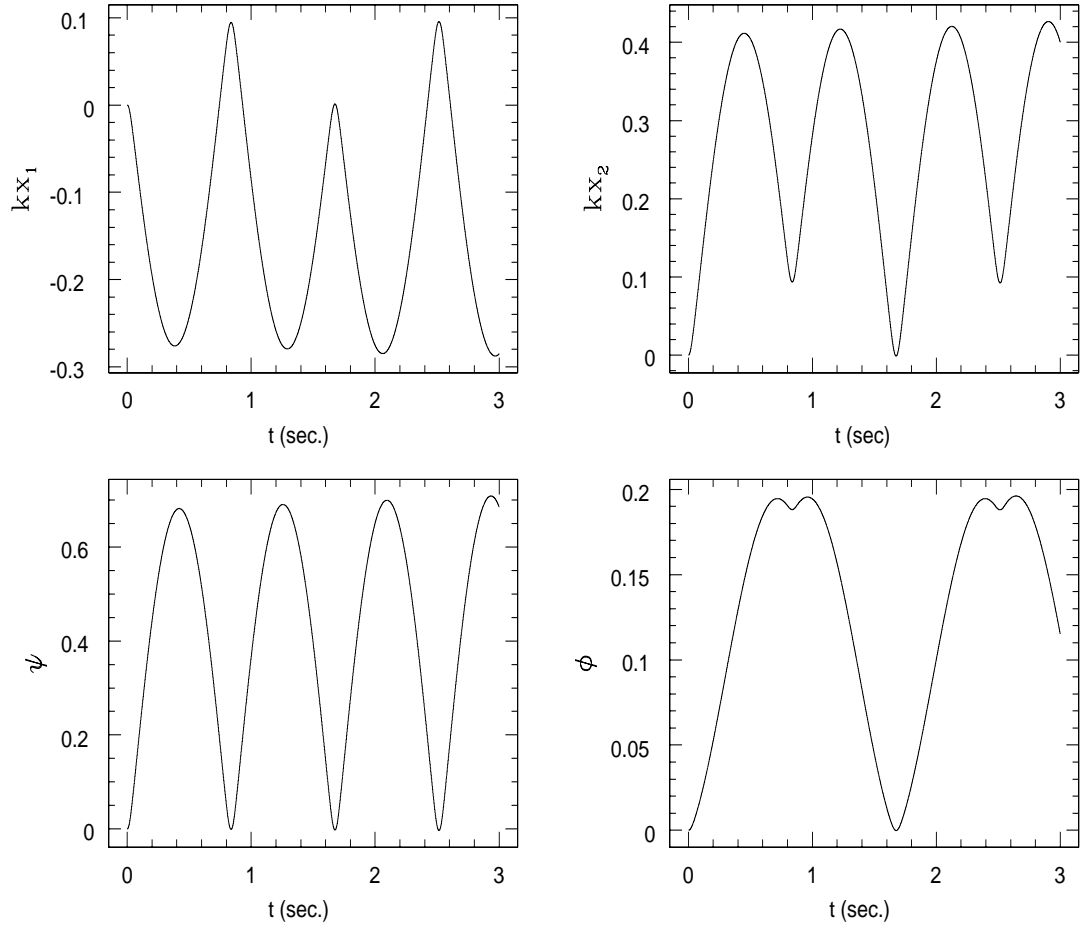


FIG. 2. Motion of the mirrors for the modes  $kx_1$ ,  $kx_2$ ,  $\psi$  and  $\phi$  as a function of time for input power of 1 kW.

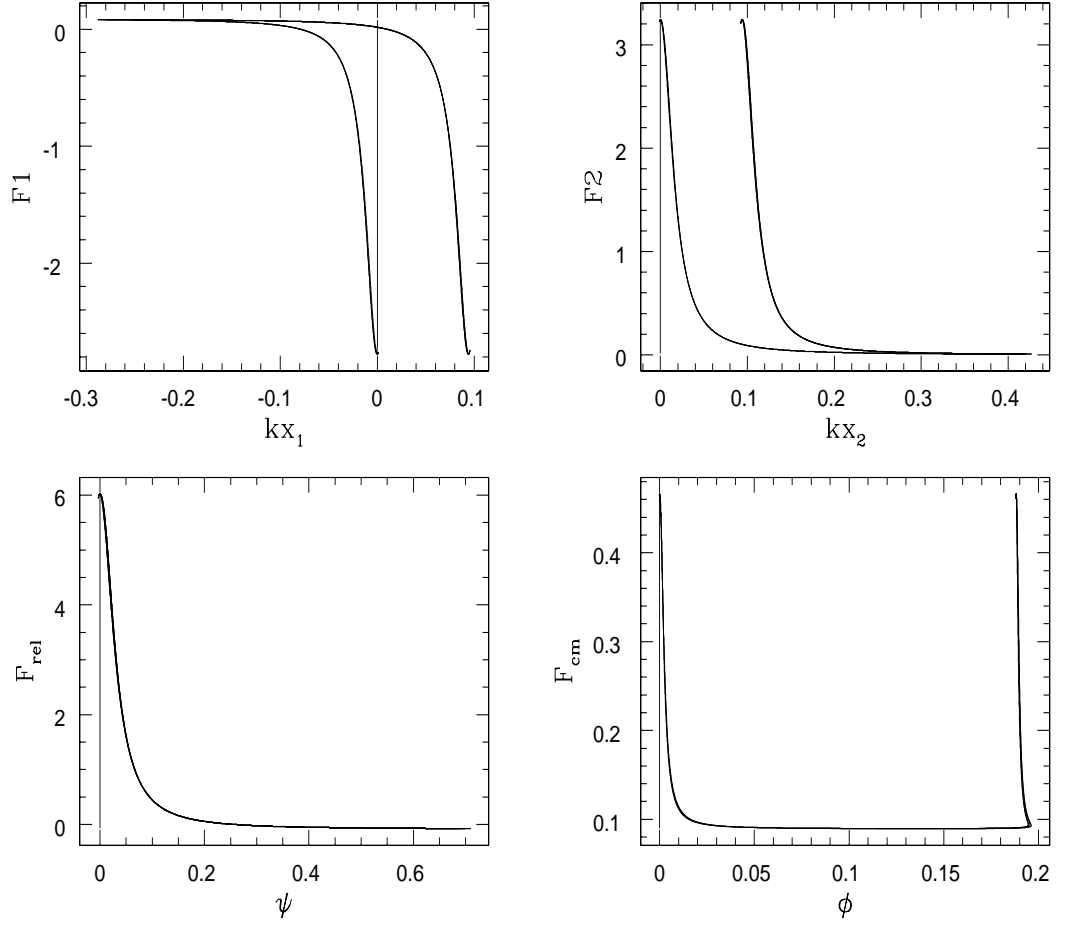


FIG. 3. Radiation pressure force profiles for the modes  $kx_1$ ,  $kx_2$ ,  $\psi$  and  $\phi$  in dimensionless units for input power of 1 kW for one cycle. The conversion factor for converting the dimensionless force into Newtons is  $m\omega^2/k$ .

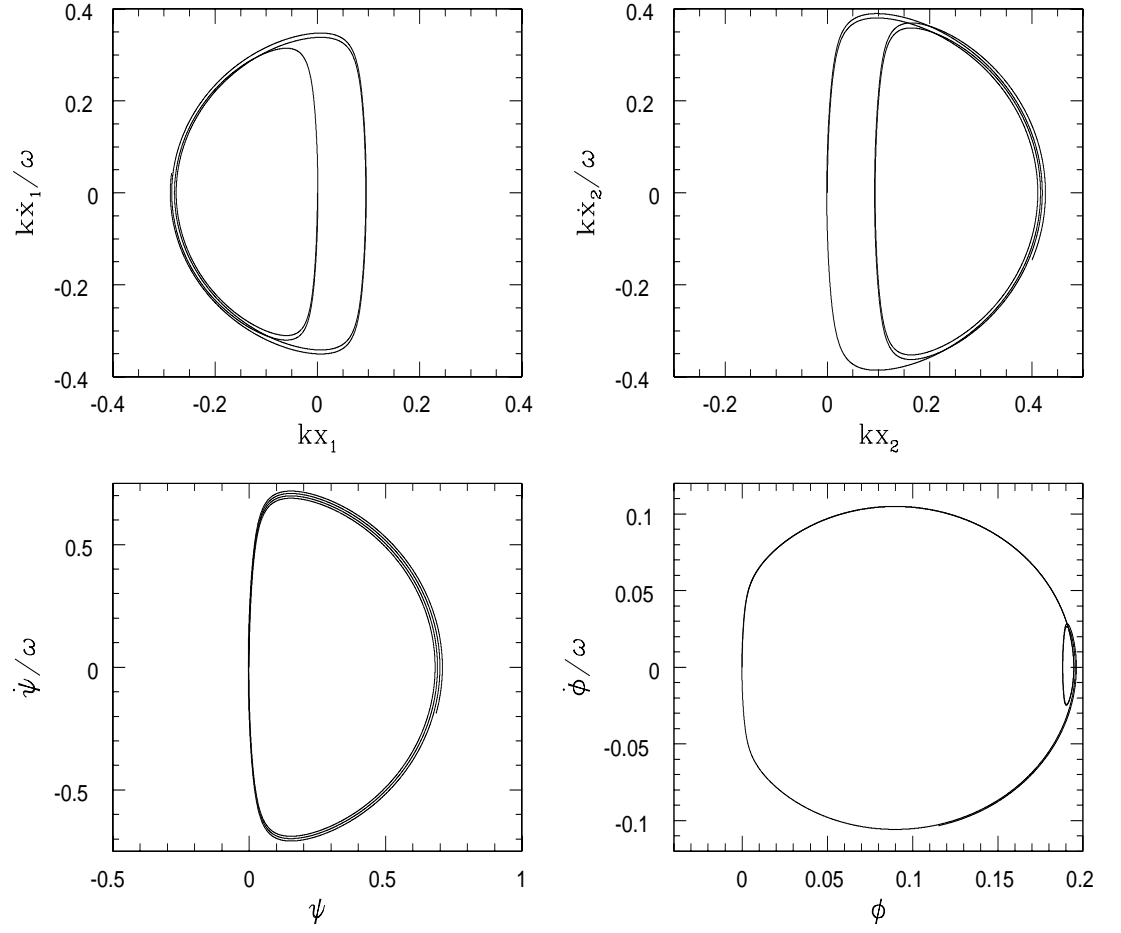


FIG. 4. Phase space diagrams for  $kx_1$ ,  $kx_2$ ,  $\psi$  and  $\phi$  for 1 kW of input power and integration time of 3 seconds.

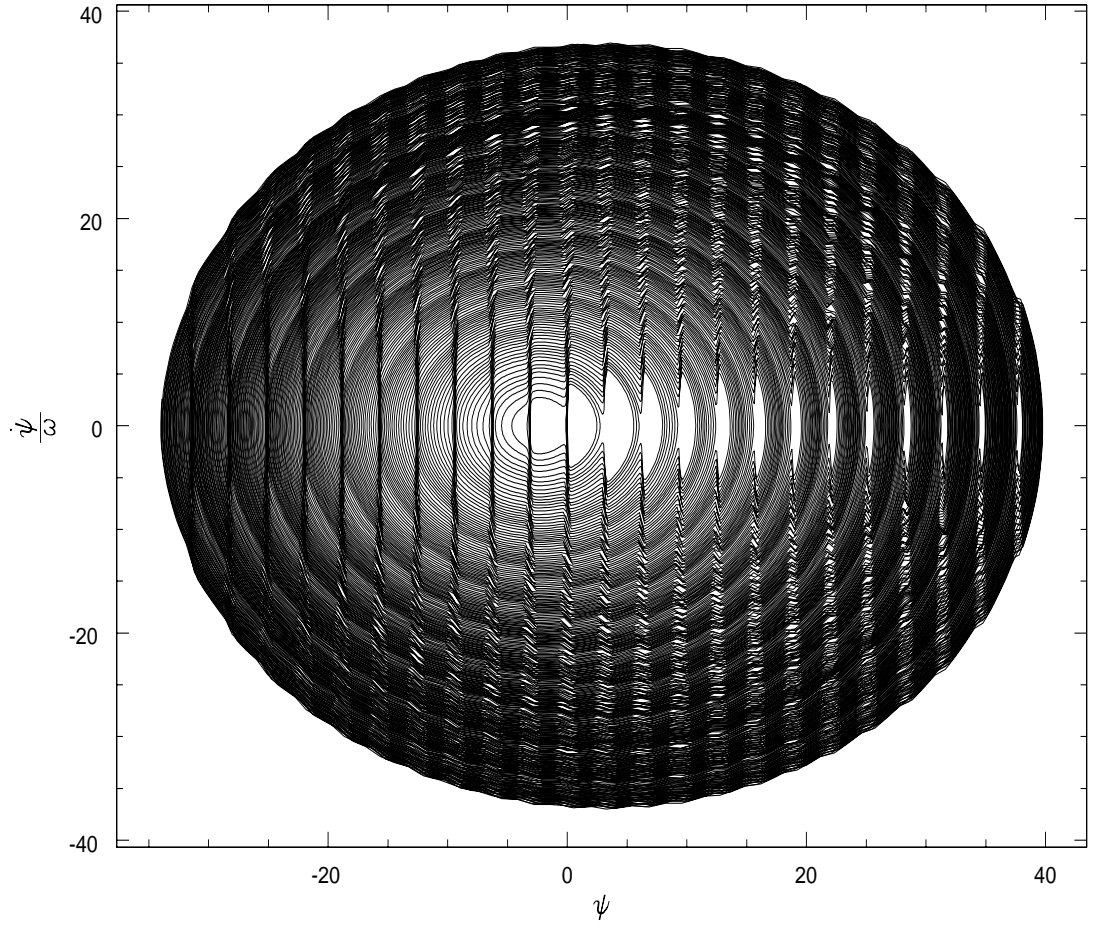


FIG. 5. Phase space diagram for  $\psi$  for the input power of 30 kW and integration time of 500 seconds.

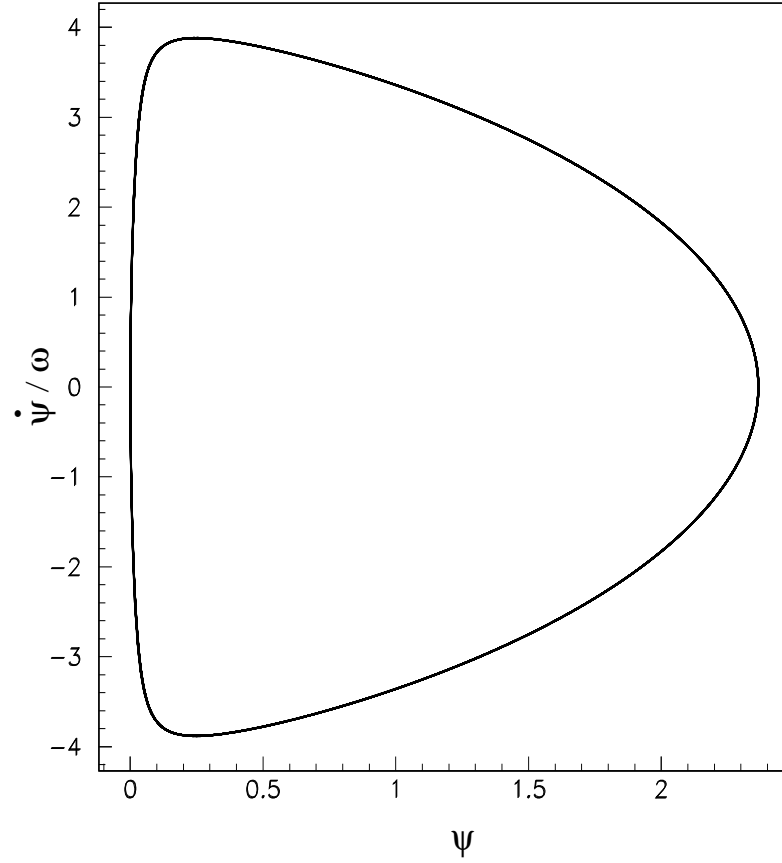


FIG. 6. Phase space diagram for  $\psi$  for the input power of 30 kW, integration time of 500 seconds and for a short cavity ( $L_0 = 30$  cm). Unlike the long cavity, studied here, there is no energy gain : the phase-space trajectory remains remarkably stable.

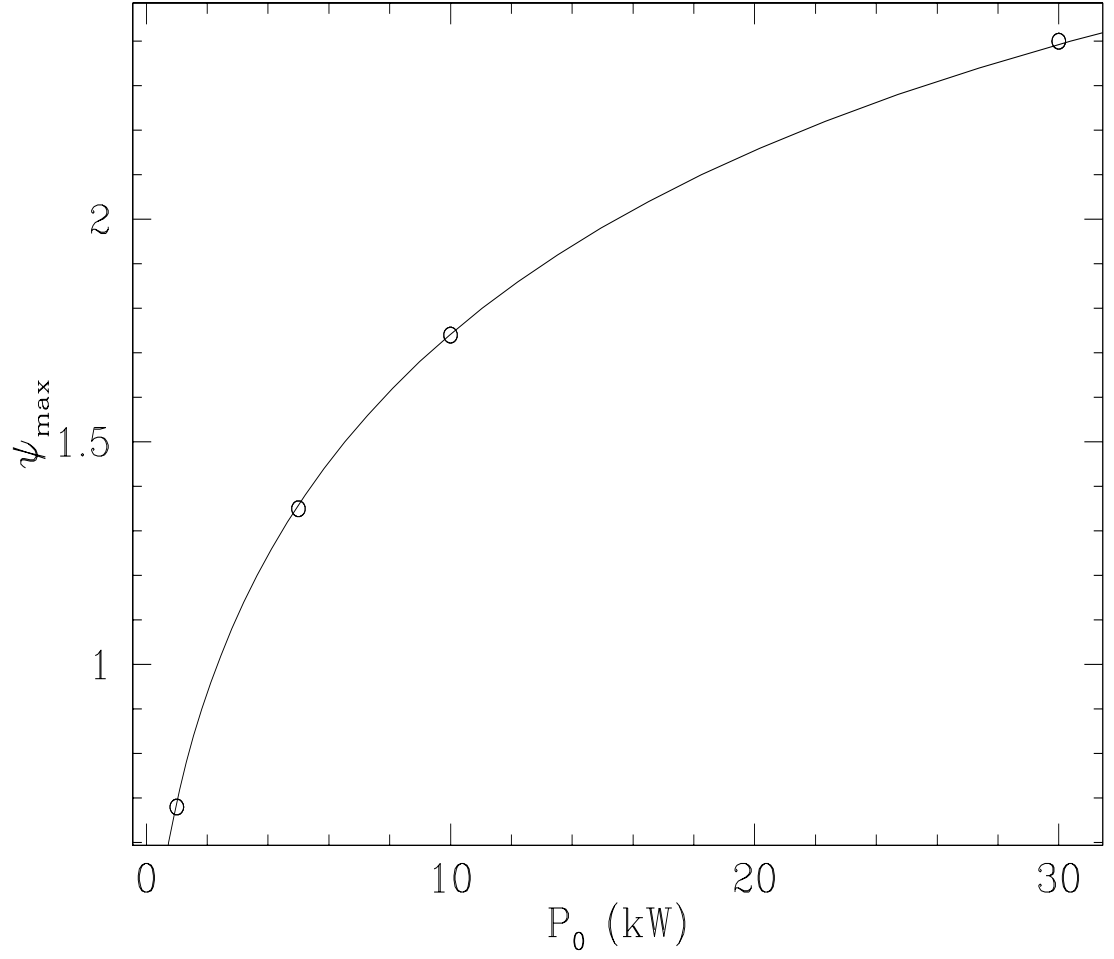


FIG. 7. Comparison of the values of  $\psi_{max}$  obtained analytically (smooth curve) and numerically (open circles) for input powers of 1 kW, 5 kW, 10 kW and 30 kW.

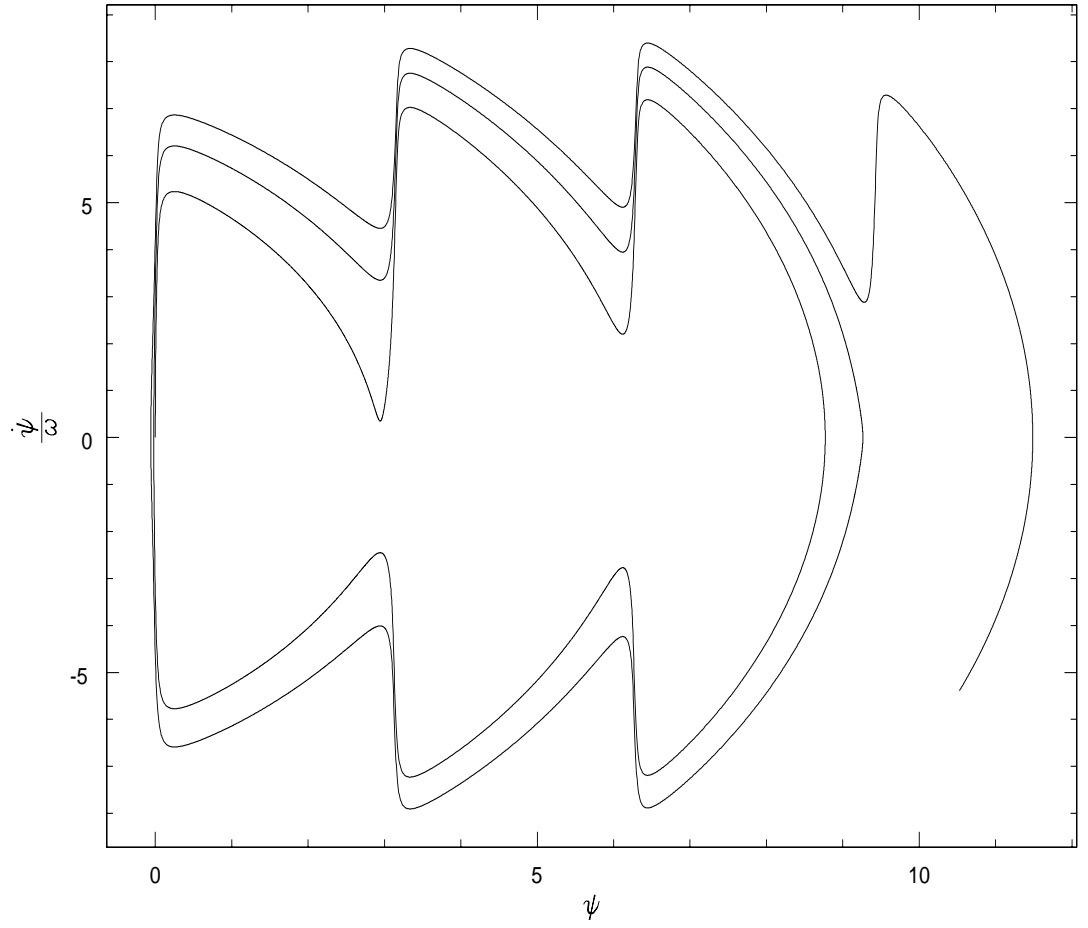


FIG. 8. Phase space diagram for the  $\psi$  mode for the input power of 50 kW and integration time of 3 seconds.



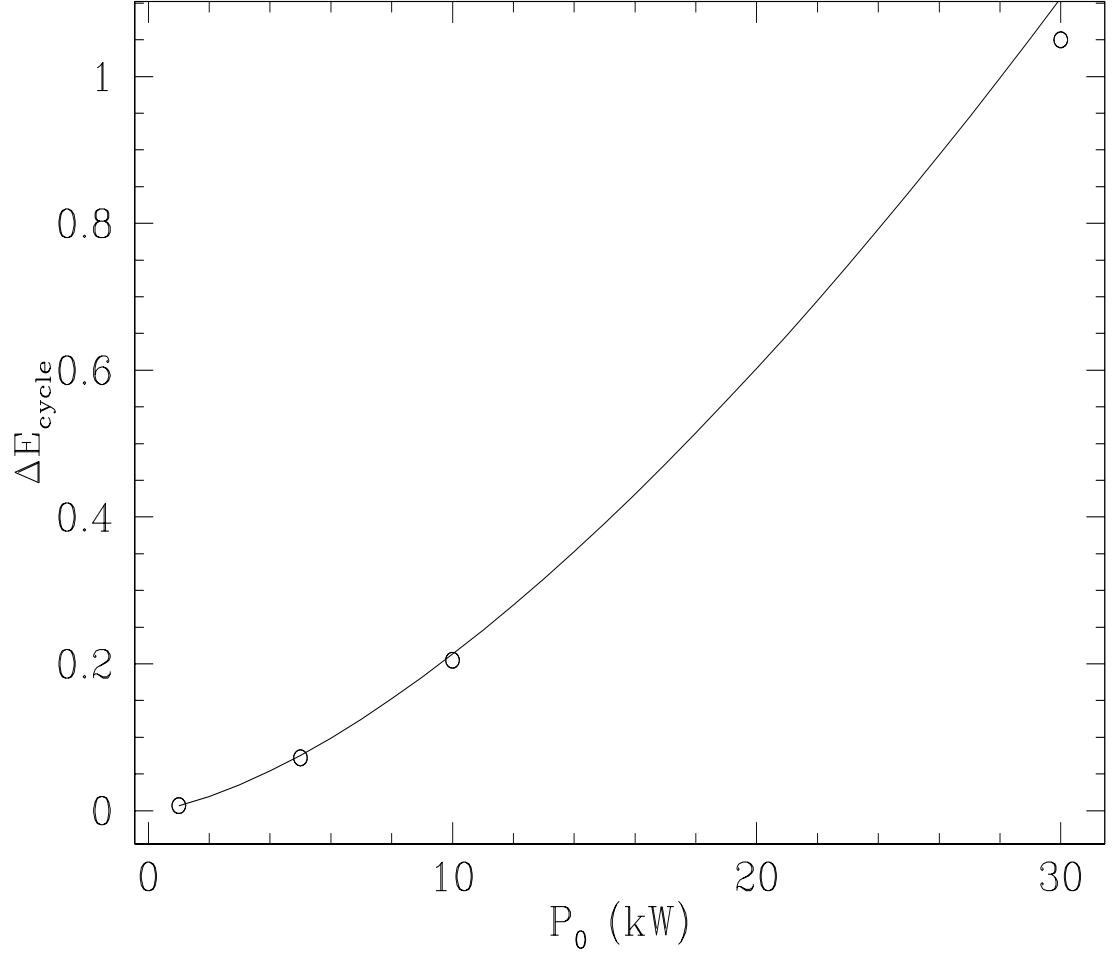


FIG. 9. The gain in energy per cycle obtained analytically (smooth curve) and numerically (open circles) for input powers of 1 kW, 5 kW, 10 kW and 30 kW. To convert the dimensionless energy gain in Joules we multiply by the factor of  $m\omega^2/k^2 \sim 11.2$  pico-Joules.

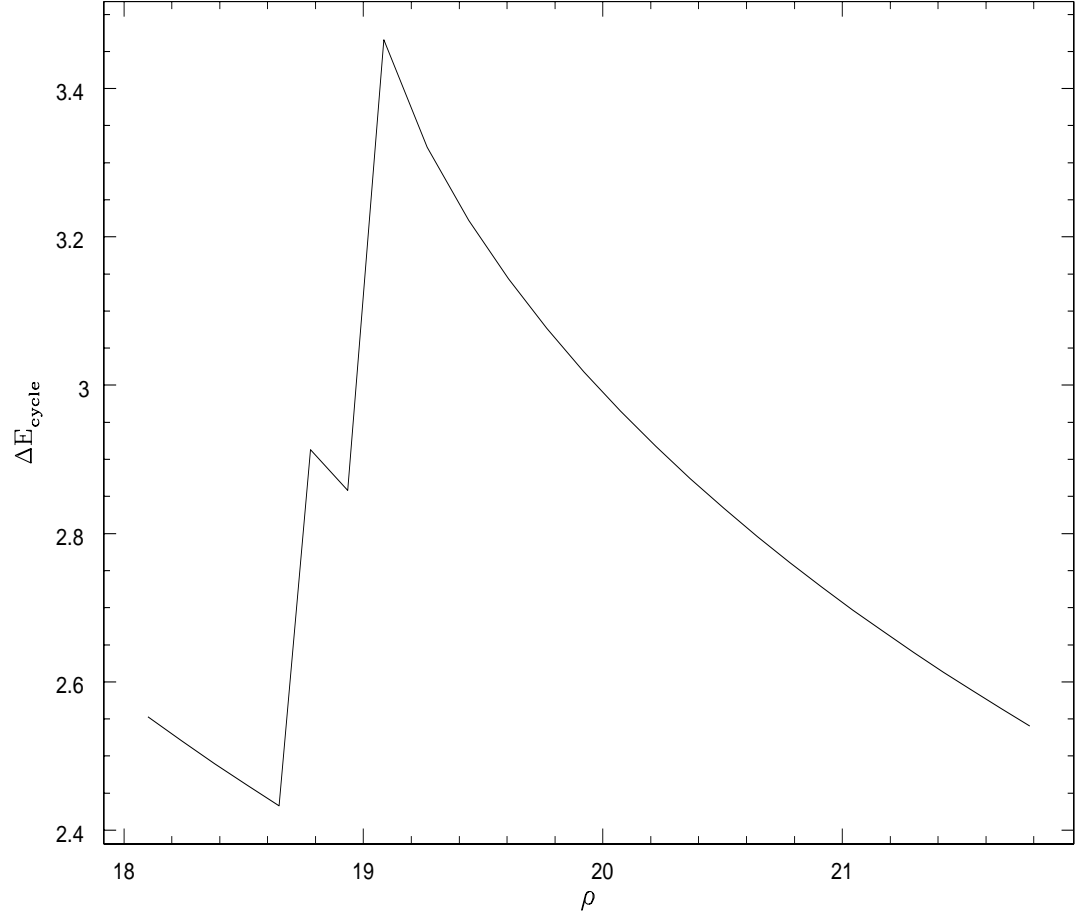


FIG. 10. The dimensionless energy gain per cycle  $\Delta E_{\text{cycle}}$  as a function of the amplitude of the  $\psi$  mode for the input power of 30 kW. The plot is analytical.

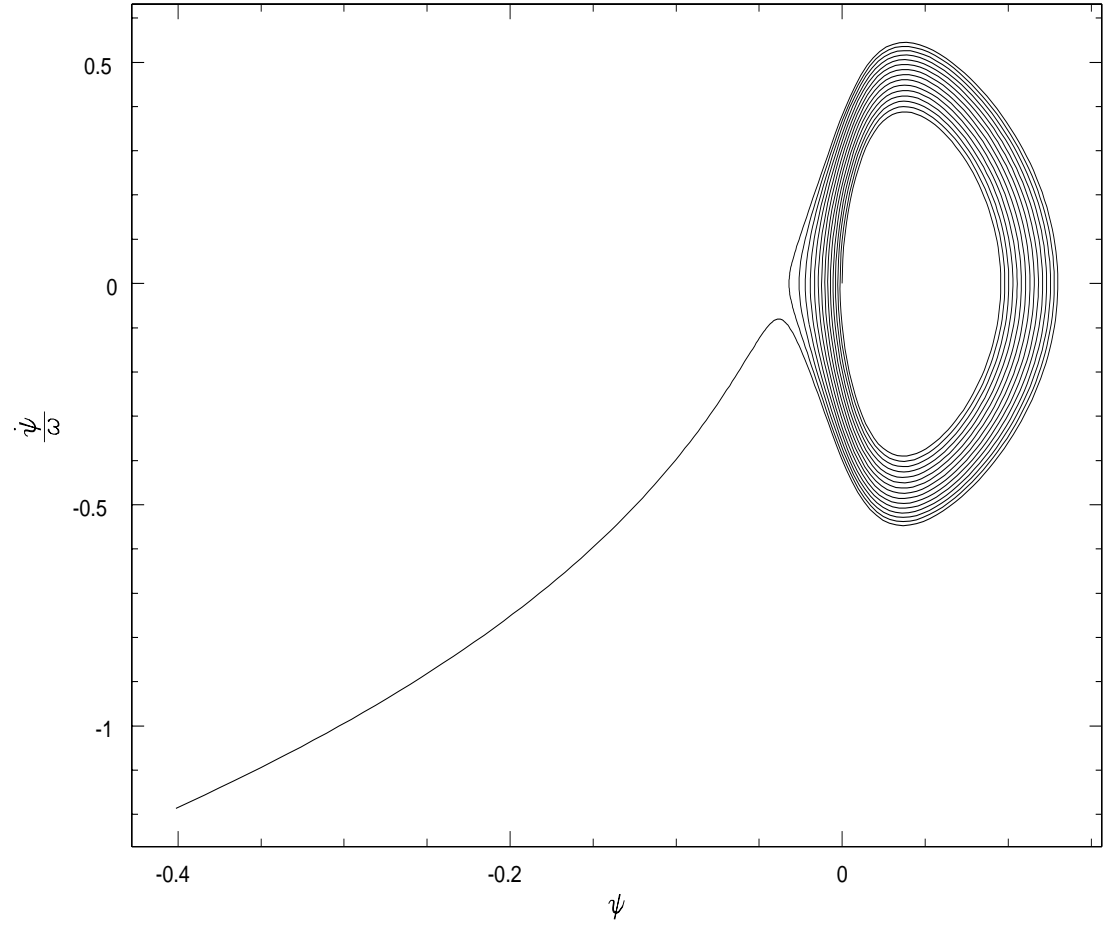


FIG. 11. The phase space diagram for the equilibrium case for the  $\psi$  mode. The input power is 1 kW and the integration time is 4 seconds.